

Compression and Decay of Hillslope Topographic Variance in Fourier Wavenumber Domain

Tyler H. Doane^{1,2} , Danica L. Roth^{3,4} , Joshua J. Roering³ , and David J. Furbish^{1,5} 

¹Department of Earth and Environmental Sciences, Vanderbilt University, Nashville, TN, USA, ²Now at Department of Geosciences, University of Arizona, Tucson, AZ, USA, ³Department of Earth Sciences, University of Oregon, Eugene, OR, USA, ⁴Now at Department of Geology and Geological Engineering, Colorado School of Mines, Golden, CO, USA, ⁵Department of Civil and Environmental Engineering, Vanderbilt University, Nashville, TN, USA

Key Points:

- Linear and nonlinear transport processes result in diagnostic behaviors in wavenumber domain
- Spectral compression and vertical spectral decay represent two end-member ways to degrade a landform
- Gaussian land-surface profiles represent a basic form and deviations from this form highlight details of transport processes

Correspondence to:

T. H. Doane,
tdoane@email.arizona.edu

Citation:

Doane, T. H., Roth, D. L., Roering, J. J., & Furbish, D. J. (2019). Compression and decay of hillslope topographic variance in fourier wavenumber domain. *Journal of Geophysical Research: Earth Surface*, 124, 60–79. <https://doi.org/10.1029/2018JF004724>

Received 20 APR 2018

Accepted 14 DEC 2018

Accepted article online 21 DEC 2018

Published online 15 JAN 2019

Abstract Three mathematical models of hillslope sediment transport are common: linear diffusion, nonlinear diffusion, and nonlocal transport. Each of these is supported by a different theory, but each contains land-surface slope as a central ingredient. As such, land-surface evolution by all three of these models is largely similar in that topographic highs degrade and lows fill in. However, details of land-surface evolution into wavenumber (Fourier) domain, which effectively separates signals into coarse- and fine-scale elements of land-surface form, such as hillslope-valley sequences and pit-mound features, respectively. In wavenumber domain linear diffusion results in vertical spectral decay, which is associated with landform straightening and smoothing of sharp concavities. Nonlinear diffusion results in spectral compression toward low wavenumbers, which is associated with landform lengthening and is similar to slope replacement. Nonlocal processes share elements of linearity or nonlinearity but are modified by the particular form of the distribution of particle travel distance. Ultimately, all processes tend toward zero topographic variance, but by distinctly different styles as revealed in wavenumber domain. Spectral compression by nonlinear processes can result in temporary spectral growth over certain spectral bands and is interpreted as a signature of nonlinear processes for certain landforms. The signatures come from the evolution of topographic details and landforms with sharp concavities highlight this behavior, whereas landforms with low concavities obscure these diagnostic behaviors.

1. Introduction

Mathematical descriptions of hillslope sediment transport are a central component of geomorphology. Formulations for sediment transport provide a tool to analyze the form of landscapes (Roering et al., 2007), identify relationships between tectonics and climate (Fernandes & Dietrich, 1997; Hughes et al., 2009; Hurst et al., 2012; McGuire et al., 2014; Perron et al., 2012), and understand the motion and spatial distribution of nutrients and organic carbon (Hales et al., 2012; Reneau & Dietrich, 1991). Three hillslope sediment transport models are common, namely, local linear diffusion, local nonlinear diffusion, and nonlocal transport. Each of these is supported by a different theory; however, they share a common foundation in that the rate of sediment transport is a function of the land-surface slope. Linear and nonlinear models describe the hillslope sediment flux as linear or nonlinear functions of the local slope. Nonlocal models describe the flux as a weighted function of surrounding slopes. Whereas mathematical distinctions between these three formulae are clear, their physical manifestations are not easily distinguished. This work is aimed at exploring potential signatures and identifying fundamental consequences of these transport formulae that are observable in land-surface evolution.

At a large scale, the slope dependencies of local linear, nonlinear, and nonlocal transport lead to an elastic evolution of topography (Schumer et al., 2017). That is, in the absence of tectonic forcing, topographic highs tend to degrade and lows tend to fill. With reference to landscape-scale applications then, all models effectively produce the same low-order morphology. If a question is aimed at a low-order description of transport or its consequences, the simplest transport model is appropriate. However, these models definitively differ in their theoretical underpinnings, and therefore, the meaning of central parameters, or the magnitude of parameters, will differ. Generally, parameters of transport formulae are rate constants that reflect the magnitude of regolith churning or the activity of particles. To obtain values for these, it is common to numerically

simulate land-surface evolution and back calculate a value that results in the best fit modeled land-surface profile (DiBiase et al., 2010; Doane et al., 2018; Fernandes & Dietrich, 1997; Madoff & Putkonen, 2016; Nash & Beaujon, 2006). However, fitting linear and nonlinear models to a single hillslope will result in different estimates of the hillslope diffusivity and will imply different magnitudes of soil churning (Doane et al., 2018), so we risk misunderstanding the mechanisms of sediment transport. Therefore, we must rely on signatures of linear, nonlinear, and/or nonlocal processes in land surface form if we are to correctly identify transport mechanisms.

At a hillslope scale, the mechanistic style of sediment transport can be distinguished in hillslope form. For example, at topographic steady state, a nonlinear formulation for the hillslope sediment flux results in a straighter profile than linear diffusion (Roering et al., 1999). Likewise, nonlocal transport can produce relatively straight profiles, depending on the formulation (Foufoula-Georgiou et al., 2010; Furbish & Haff, 2010; Tucker & Bradley, 2010). Whereas these geometric qualities are helpful and clearly stated, topographic steady state is a rare condition. Nonetheless, the recognition that slopes become uniform with distance downslope under certain geomorphic conditions highlights the idea that the details of the land surface contain evidence of the mechanistic style of sediment transport. This work explores the evolution of the details of the land surface in a transient setting and identifies clear diagnostic behaviors for a set of initial and boundary conditions.

To observe the details of the land surface, it is helpful to transform it into the wavenumber representation via the Fourier transform. Previous authors have demonstrated the value of using the Fourier transform for Earth surface applications to identify characteristic length scales (Perron et al., 2008), evaluate the surface roughness (Booth et al., 2017), and solve advection-diffusion equations (Ganti et al., 2010; Schumer et al., 2009). Here we use the Fourier transform of landforms to identify the high and low-order structure which refers to the more and less detailed elements of the land surface. We elaborate on a distinction between high- and low-order structure and provide a working definition later. We suggest that clues to the physics of sediment transport are contained in the evolution of a small portion of topographic variance that is represented by the higher-order structure of topography.

We provide a detailed look at land-surface evolution in wavenumber domain. Work demonstrating nonlocal transport in a natural setting identified previously unreported land-surface behavior in wavenumber domain (Doane et al., 2018). The observation warrants a closer look at evolution in wavenumber domain; however, the potential for signatures of nonlocal transport is an additional motivator. The inherent length scale involved with nonlocal transport and the ability for wavenumber domain to highlight latent length scales suggests that information of the particle travel distances might be revealed. The theory presented below does not highlight a unique signature of nonlocal transport or provide clear information on particle travel distances. It does, however, illuminate behaviors of linear and nonlinear processes.

We identify two distinct behaviors of linear and nonlinear processes. In wavenumber domain, theory shows that linear diffusion leads to vertical destruction of spectral amplitude at rates that scale with wavenumber (Schumer et al., 2009). We show here that nonlinear processes tend to compress the spectrum into lower wavenumbers, and in doing so, the spectrum tends toward longer wavelength features. In this paper, these styles of spectral evolution represent two end-member styles to quash topographic variance. We present theory that explains the spectral evolution according to linear, nonlinear, and nonlocal processes and address the idea of using the spectra as a tool to identify linear, nonlinear, and nonlocal processes. Spectral evolution styles are more diagnostic for certain topographic configurations, and we identify topographic characteristics that result in clearly diagnostic behaviors. We emphasize that observation of these signatures does not require any numerical modeling so they serve as a relatively simple way to observe linear or nonlinear behavior in the transport process. Numerical models that are presented below are intended to be illustrations of the theory.

This paper is organized as follows. In section 2, we briefly review the theoretical development of local linear, nonlinear, and nonlocal transport. This is covered in previous work (Culling, 1963; Fernandes & Dietrich, 1997; Furbish & Haff, 2010; Furbish & Roering, 2013; Roering et al., 1999), so we cover the basic principles here. Section 3 introduces the Fourier transform and applies the theory of land-surface evolution in wavenumber domain. In section 4 we present an experimental analogue involving acoustically stimulated simulation of land-surface evolution that highlights spectral evolution according to nonlinear sediment

dynamics. Last, we present case studies of examples from the natural landscapes with simple topographic configurations.

2. Sediment Transport Theory

2.1. Linear Diffusion

Linear diffusion has a long legacy in geomorphology (Carson & Kirkby, 1972; Culling, 1965; Fernandes & Dietrich, 1997; Furbish & Fagherazzi, 2001; Jyotsna & Haff, 1997; Putkonen et al., 2008). Culling (1963) suggested that the quasi-random creation and collapse of pore space within a soil column drives bulk downslope motion. The rate of bulk motion scales linearly with land-surface slope as the lofting motions are, on average, normal to the land-surface slope and settling motions are, on average, down (Furbish et al., 2009). The volumetric hillslope sediment flux, $q(x)$ [$L^2 T^{-1}$], is often described as

$$q(x) = -D \frac{d\zeta}{dx}, \quad (1)$$

where D [$L^2 T^{-1}$] is a diffusivity-like rate constant, ζ [L] is the land-surface elevation, and x [L] is a horizontal position. Placing (1) into the Exner equation returns the familiar diffusion equation

$$\frac{\partial \zeta}{\partial t} = D \frac{\partial^2 \zeta}{\partial x^2}. \quad (2)$$

Mathematical treatment of (2) is extensive (Carslaw & Jaeger, 1959; Hornberger & Wiberg, 2013; Schumer et al., 2009).

2.2. Nonlinear Diffusion

Whereas (1) captures the basic idea that sediment flux varies with slope, there is evidence that the relationship between land-surface slope and sediment flux is nonlinear (Roering et al., 1999). For example, landscapes such as the Oregon Coast Range that are in an approximate steady state condition contain hillslopes whose profiles become increasingly straight with distance from the divide (Roering, Kirchner, & Dietrich, 2001). This condition suggests that with increasing slope, the hillslope sediment flux must increase nonlinearly such that the divergence of the flux remains constant to satisfy the steady state condition.

Treatment of frictional and gravitational forces acting on soil as a function of slope (Roering et al., 1999) leads to a nonlinear functional form for the sediment flux

$$q(x) = -D \frac{S}{1 - \left(\frac{|S|}{S_c}\right)^2}, \quad (3)$$

where S is the land-surface slope and S_c is a critical slope related to the friction slope. This formulation suggests that as slopes steepen friction is increasingly ineffective and surface processes such as dry ravel and small landslides occur more frequently. Equation (3) effectively accounts for observed topographic and erosion rate data that show a nonlinear relationship between slope and hillslope sediment flux (Gabet, 2000, 2003; Roering et al., 1999, 2007).

2.3. Nonlocal Transport

The class of nonlocal models is largely motivated by the success of nonlinear diffusion. To generate large fluxes, nonlinear flux formulations appeal to an increase in pace of particle motions (e.g., tree throw, dry ravel, and shallow landslides), yet it does not include a description of particle travel distances. Travel distances associated with these motions can be on the order of meters if not tens of meters (DiBiase et al., 2017; Gabet & Mendoza, 2012), yet (3) is a local function of x . That the expression is local but invokes nonlocal motions implies that (3) is an incomplete treatment of transport (Doane et al., 2018). Nonlocal models explicitly address this concern. Furthermore, local nonlinear models are inherently scale dependent and applicable only at resolutions greater than the roughness scale (i.e., scales associated with biogeomorphic roughness) whereas nonlocal models can be scale independent (Ganti et al., 2012).

Three general models incorporate nonlocality. Fractional calculus models take advantage of a noninteger derivative of a quantity, which produces a nonlocal dependence (Foufoula-Georgiou et al., 2010). A rule-based model that evaluates the probability of continued motion for a parcel of sediment based on the local topographic conditions leads to long-distance motions (Tucker & Bradley, 2010). Last, a probabilistic model involves the convolution of a volume of sediment set in motion around x with the probability that the

sediment passes through x (Furbish & Haff, 2010; Furbish & Roering, 2013). Here we will focus on a convolution integral form because the ingredients, a volumetric entrainment rate and particle travel distance, are well-defined quantities that are, in principle, measurable (DiBiase et al., 2017; Gabet & Mendoza, 2012; Kirkby & Statham, 1975).

A convolution integral formulation for nonlocal hillslope sediment transport is (Doane et al., 2018; Furbish & Haff, 2010; Furbish & Roering, 2013),

$$q(x) = \int_0^x E(x')R(x - x', x')dx', \quad (4)$$

where $x = 0$ is the ridge-top location, x' is an upslope position, $E [L^3 L^{-2} T^{-1}]$ is a volumetric entrainment rate, and R is like a kernel, and it is the survival function of particle travel distance. This is not a true convolution because the parameters of the survival function of travel distance, $R(x - x', x')$, are allowed to change with x' as the slope changes, and therefore, R is not a true kernel (Gilad & von Hardenburg, 2006). That is, the mean travel distance increases with slope such that probability is shifted toward the tail of the distribution of travel distances. The survival function describes the probability that particles travel at least a distance $x - x'$, which implies that they contribute to the flux. There may be different functional forms for both $E(x')$ and $R(x - x', x')$ that depend on the suite of processes that occur in a given region. Land-surface slope, however, is often a central variable in both functions, which provides a linear or nonlinear slope dependency. Therefore, behaviors of a nonlocal formulation can be similar to both linear and nonlinear transport depending on how the entrainment rate and survival function are formulated (Doane et al., 2018).

The three mathematical forms are all physically based models of sediment transport and linear or nonlinear forms reflect bulk motion due to different processes. For example, the sediment flux due to transport by rain splash is linearly related to land-surface slope (Furbish et al., 2009), whereas transport due to dry ravel varies nonlinearly with land-surface slope (Gabet, 2003). Although sediment transport definitively occurs by a number of different physical mechanisms, the physical signatures of mechanisms are subtly recorded in topography. Below we explore the representation of these models in wavenumber domain to understand possible signatures.

3. Land-Surface Evolution in Wavenumber Domain

To illustrate distinctive behaviors of transport formulae in wavenumber space, we rely on the identities of the Fourier transform. By definition, the Fourier transform of a function $f(x)$ (i.e., land-surface elevation) of position x is

$$\hat{f}(k) = \int_{-\infty}^{\infty} f(x)e^{-ikx}dx, \quad (5)$$

where $\hat{f}(k)$ is spectral amplitude [L^2] and $k [L^{-1}]$ is wavenumber ($k = 2\pi/l$, radians per unit distance where l is wavelength). We emphasize that this is the *spectral amplitude* and not the *spectral power*, which would be the amplitude squared. In this case, the spectral amplitude carries units of L^2 because it is a transform over space, therefore integrating elevation over position. Fourier transforms have a convenient property that states that a convolution of two functions in arithmetic space is multiplicative in wavenumber domain,

$$\int_{-\infty}^{\infty} f(x')g(x - x')e^{-ikx'}dx' = f(x) * g(x) = \frac{1}{2\pi}\hat{f}(k)\hat{g}(k), \quad (6)$$

where the asterisk denotes a convolution. Additionally, the representation of a derivative (using Einstein notation $\frac{df}{dx} = f_x$) in configuration space is straightforward in wavenumber domain,

$$\hat{f}_x(k) = ik\hat{f}(k). \quad (7)$$

The Fourier transforms of higher-order derivatives are simply ik raised to the integer order of the derivative. For example, the transform of a second derivative with respect to position is

$$\hat{f}_{xx}(k) = (ik)^2\hat{f}(k). \quad (8)$$

Einstein notation is used in this manuscript only when referring to derivatives in wavenumber domain; otherwise, Leibniz notation for derivatives is adopted.

In this section we explore the impacts of different transport formulae on the evolution of the elevation spectra. We conduct the analysis in the context of simple topographic configurations to illustrate the behavior. To simplify the analysis in wavenumber domain, we reflect landforms about the origin such that their graphical representation is an even function (symmetric about the origin), and therefore, the transform is real. The rules presented above allow for (2)–(4) to be recast as their transforms, and land-surface evolution can be described in wavenumber domain for a set of topographic configurations. From this analysis, different behaviors emerge that highlight the evolution of high-order topographic structure. These analyses, although strictly applicable to the set of landforms tested, broadly identify land-surface behaviors that correspond with linear, nonlinear, and nonlocal models.

3.1. Linear Diffusion

Mathematical treatment of partial differential equations like (2) is extensive and previous work has identified an analytical expression for the time evolution of a quantity undergoing linear diffusion (Carslaw & Jaeger, 1959; Schumer et al., 2009). Using (8),

$$\hat{\zeta}_t(k) = -Dk^2\hat{\zeta}(k). \quad (9)$$

This result is particularly significant, as it indicates that spectral amplitude in all wavenumbers must decay with time. The rate of decay scales with wavenumber such that low wavenumber (long wavelength) features persist longer than large wavenumber (short wavelength) features. Separating variables and integrating with respect to t yields an analytical solution for the transient evolution of the Fourier transform of the land-surface elevation (Carslaw & Jaeger, 1959; Mudd & Furbish, 2007; Schumer et al., 2009)

$$\hat{\zeta}(k, t) = \hat{\zeta}(k)e^{-k^2Dt}. \quad (10)$$

That topography decays exponentially in the absence of external forcing (i.e., tectonics) has been exploited for various applications (Booth et al., 2017; Mudd & Furbish, 2007) and is a well-known behavior.

3.2. Nonlinear Diffusion

In contrast to (9), there is no simple expression for the time evolution of the Fourier transform of a profile evolving according to nonlinear diffusion. To investigate the influence of nonlinear terms, we add a nonlinear term to (1). For illustration, we consider a single nonlinear term that has slope raised to a power of three,

$$q(x) = -D_1 \left(\frac{d\zeta}{dx} \right)^3 - D_0 \frac{d\zeta}{dx}, \quad (11)$$

where D_0 and D_1 [$L^2 T^{-1}$] are diffusivity-like rate constants. We write the flux this way for two reasons. First, an odd power on slope maintains the correct dependence on the sign of the slope such that negative slopes have positive fluxes. Second, when $D_0/S_c^2 = D_1$, the expression is equal to the first two terms in the Taylor expansion of (3) (Doane et al., 2018; Ganti et al., 2012) and therefore is capable of capturing the basic behavior of a physically based nonlinear formulation. Placing (11) into the Exner equation yields

$$\frac{\partial \zeta}{\partial t} = 3D_1 \left(\frac{\partial \zeta}{\partial x} \right)^2 \frac{\partial^2 \zeta}{\partial x^2} + D_0 \frac{\partial^2 \zeta}{\partial x^2}. \quad (12)$$

Note that in the absence of the second term on the right-hand side of (12), there is no change in elevation at ridges that have zero slope but finite concavity. This result would be unrealistic, and therefore, a linear diffusion term is required.

The Exner equation in the form of (12) can be recast in wavenumber domain using the properties of Fourier transforms presented above. In particular, we take advantage of the inverse of the convolution theorem for Fourier transforms so that

$$\hat{\zeta}_t(k) = \frac{3D_1}{4\pi^2} \hat{\zeta}_{xx}(k) * [\hat{\zeta}_x(k) * \hat{\zeta}_x(k)] - D_0 k^2 \hat{\zeta}(k), \quad (13)$$

where the asterisk denotes a convolution and subscripts on the transforms indicate a transform of a derivative. The form of (13) can be summarized mathematically as a convolution of the Fourier transform of slope with itself, which is then convolved with the transform of concavity. That the time derivative involves

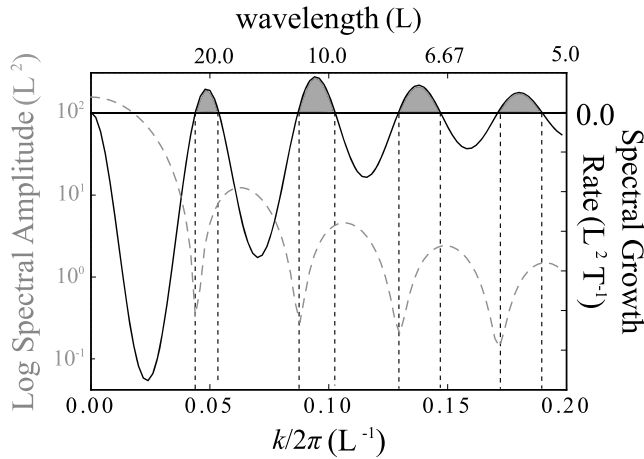


Figure 1. Plots of the spectral amplitude of a triangle (dashed gray line), $\hat{\zeta}(k)$, and the spectral growth rate (black line), which results from a local nonlinear flux formulation. Growth rates here are calculated for the initial evolution of a triangle after a short amount of time. Regions of positive growth rates are highlighted in gray and are offset from the peaks in the elevation spectrum.

3.3. Nonlocal Transport

The convolution integral in nonlocal formulations is the principal element distinguishing it from local linear or nonlinear diffusion. Here we highlight the impact of a convolution integral on the evolution of elevation spectra. To do so, we must consider a simplified topography for which the flux is positive everywhere and has a relatively linear slope (e.g., river terrace riser). The linear slope is important here because we cannot allow the survival function, $R(x - x', x')$, to vary with position. This is so that the dependency on x' is removed and the kernel is consistent across space, which allows for the convolution theorem for Fourier transforms to be applied. With these assumptions in place, we can use the properties of the Fourier transform to illuminate the essential effect of a convolution.

Using the convolution theorem for Fourier transforms and the rules for derivatives, we write the Exner equation in wavenumber domain as

$$\hat{\zeta}_t = -ik\hat{E}\hat{R}, \quad (14)$$

where \hat{E} is the transform of the volumetric entrainment rate, $E(x')$, and \hat{R} is the transform of the survival function, $R(x - x')$, of travel distance. Previous work has suggested that most particles travel short distances while fewer travel far, which is a characteristic of exponential distributions (Doane et al., 2018; Furbish & Haff, 2010; Furbish & Roering, 2013). For an exponential distribution with survival function $R(x - x')$,

$$\hat{\zeta}_t = -ik\hat{E}\frac{\mu_x}{1 + ik\mu_x}, \quad (15)$$

where μ_x is the mean travel distance on the given slope. Note that \hat{R} contains real and imaginary parts (Figure 2), and therefore, a general behavior is not easily determined and depends on form of the land-form. However, we can highlight the impact that μ_x has on land-surface evolution.

Imagine a terrace, with the midpoint of the slope centered at the origin (Figure 3). The slope of the land-surface is then a boxcar function centered at the origin. This condition satisfies our requirement that $R(x - x', x')$ be invariant with x' for the sloped part. Let us suggest that $E = E_1 S$, such that E is an even function and $\hat{E}(k)$ contains only real parts. In this

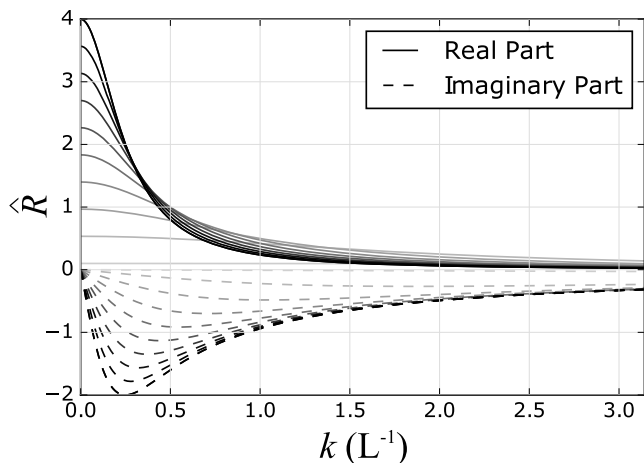


Figure 2. Plot of real and imaginary parts of $\hat{R}(k) = \frac{\mu_x}{1 + ik\mu_x}$ for $\mu_x = 0.1$ to $\mu_x = 4.0$. Lighter colors correspond with smaller values of μ_x .

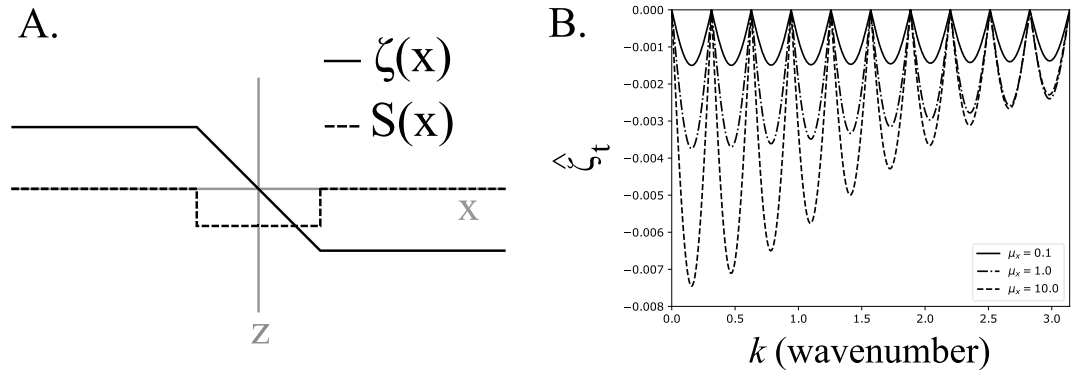


Figure 3. (a) Plots of land-surface elevation and land-surface slope for a terrace centered on the origin. (b) Plots of $\hat{\zeta}(k, 0)$ (gray) and spectral growth rates for different values of μ_x .

case, spectral amplitude in all wavenumbers decay, but at a rate that differs from that of linear diffusion (Figure 3) as shown by the different forms of $\hat{\zeta}_t$ with different values for μ_x . This illustrates the behavior of the land-surface spectra as a result of convolution and that longer travel distances more rapidly reduce the spectral amplitudes at low wavenumber (Figure 3b).

A nonlocal formulation is a convolution integral that weights the impact of x' on the flux at x based on the distance, $x - x'$, with generally more weight applied to nearby locations. This is like a low-pass filter applied to the entrainment rate, which is a function of topography. By definition, low-pass filters effectively remove high-wavenumber features so that nonlinearity in the relation of mean travel distance and with slope has a subtle signature in topography. As such, we expect nonlinearity in nonlocal formulations to mostly reflect the slope dependency of the entrainment rate with a minor impact from the distribution of travel distance.

We demonstrate this idea by numerically simulating the evolution of a lateral moraine according to three different nonlocal models with three different functional forms (Figure 4). First, Case A, a nonlocal model with a slope-dependent entrainment rate but uniform mean travel distance illustrates a linear nonlocal model. Second, Case B, is a model with linearly slope dependent volumetric entrainment rate with a nonlinearly slope-dependent mean travel distance. Previous work uses a Taylor expansion as a local approximation of Case B and shows that the flux according to this formulation is mildly nonlinear, with $q \approx S^{3/2}$ (Furbish & Haff, 2010). Third, Case C, a nonlinear entrainment rate and a nonlinearly slope-dependent mean travel distance illustrate strongly nonlinear behavior. With increasing nonlinearity in the volumetric entrainment rate, we observe increasing spectral compression. Given the low-pass filter argument above and results from previous work which suggests that the hillslope sediment flux is most sensitive to the entrainment

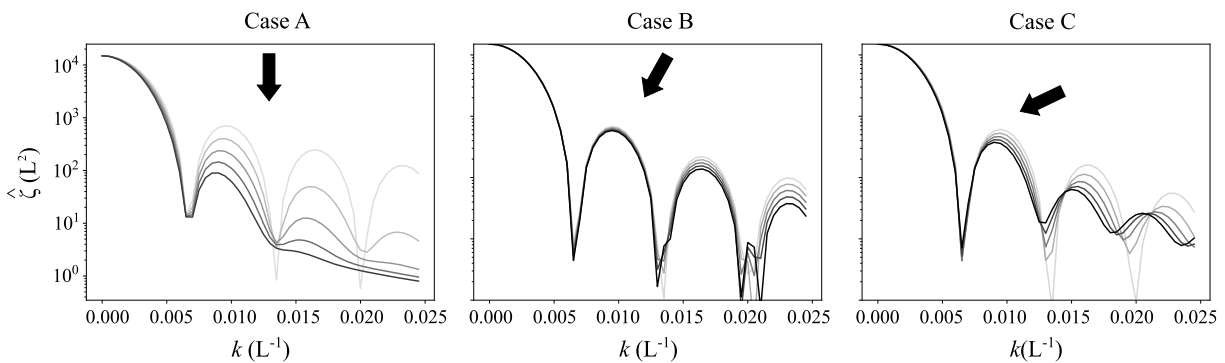


Figure 4. Spectra of land-surface profiles evolving according nonlocal models that are linear, modestly nonlinear, and strongly nonlinear. Case A: $E = E_1 S$, $\mu_x = \lambda_0$; Case B: $E = E_1 S$, $\mu_x(x) = \lambda_0 [(Sc + S)/(Sc - S)]$; Case C: $E = E_0 + E_1 S^2$, $\mu_x(x) = \lambda_0 [(Sc + S)/(Sc - S)]$. Where E_0 are background uniform entrainment rates, E_1 is a slope-modulating entrainment rate, λ_0 is a mean travel distance on a flat surface, and S_c is a critical slope similar to the friction slope. Numerical simulations were run for 50,000 iterations each with each 10,000th shown. Lighter colors indicate older profiles. Arrows are graphic illustrations of linear to strongly nonlinear behavior. Linear behavior is characterized by vertical spectral decay (represented by vertical arrow), and nonlinear behavior is characterized by spectral compression (represented by more horizontal arrows). That is, increasingly horizontal arrows represent increasingly nonlinear transport.

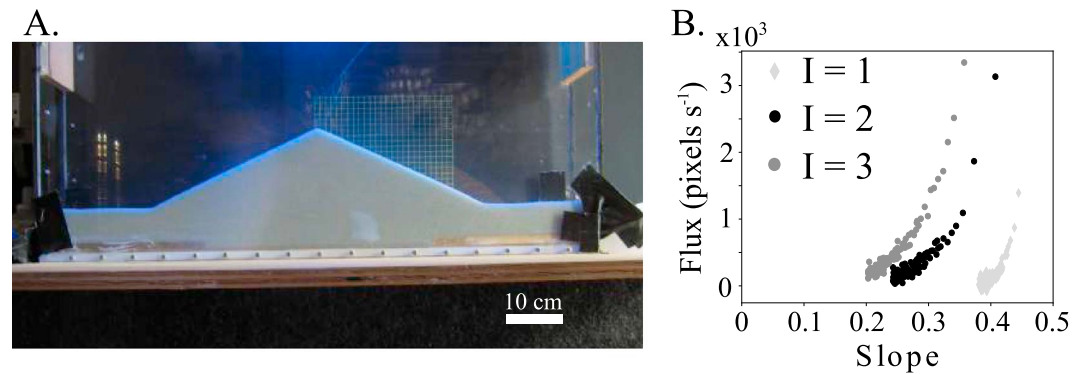


Figure 5. (a) Photo showing the experimental setup. (b) A plot of the volumetric flux versus slope. The flux here was calculated by integrating the difference between successive profiles. The noise in these plots are due to errors in profile extraction, averaging slope over long distances, and averaging slopes between successive photos. Photos were taken every 5 s and three volumes are represented by different intensities as I . Compare with Figure 1A of Roering, Kirchner, Sklar, and Dietrich (2001).

rate (Doane et al., 2018), we interpret strongly nonlinear behavior as a signature of nonlinearity in the entrainment rate.

3.4. Summary of Behaviors

We review the three basic behaviors for linear and nonlinear diffusion and nonlocal transport in wavenumber domain. First, linear diffusion results in spectral evolution in which spectral amplitudes at all wavenumbers, k , decay at a rate proportional to the amplitude and k^2 . We classify this as vertical spectral decay because it diminishes spectra locally. Second, nonlinear processes involve convolutions of functions related to the land-surface spectrum. For the landforms tested here and those that lack a moving boundary at their base, this operation tends to migrate spectral amplitude to lower wavenumber, which we classify as compressional spectral decay. For certain landforms, spectral compression temporarily results in amplitude growth in certain bands of wavenumbers, which is interpreted as a distinct signature of nonlinear processes. We emphasize that nonlinear processes do not universally lead to positive spectral growth rates. This signature only occurs when the amplitude spectra of the initial condition satisfy certain criteria that we explore below. Last, we have shown one behavior for a nonlocal formulation with a linear slope dependency, which is characterized by vertical spectral decay—although with a different dependency on the wavenumber k than linear diffusion. Previous work shows that nonlocal formulations are capable of resulting in compressional spectral decay (Doane et al., 2018) when the entrainment rate is nonlinearly related to slope. There is no clear signature of length scales of transport that emerge from wavenumber domain. However, spectral migration or vertical decay will occur according to the nonlinearity of a nonlocal formulation. Vertical spectral decay occurs when there is only a slope dependency on the distribution of particle travel distance. Mild spectral compression occurs when there is a linear slope dependency for volumetric entrainment rate and a slope-dependent mean travel distance. Strong spectral compression occurs when the volumetric entrainment rate is nonlinear and the mean travel distance is slope dependent as well.

The following sections examine the evolution of an experimental hillslope and three different topographic configurations. These landforms were selected because they have known initial and boundary conditions so we can infer their evolution and observe the signatures described above. The combination of these signatures with field evidence can suggest something about the mechanisms of transport. For example, on certain landforms with suitable boundary conditions and known initial conditions, we observe evidence of nonlocal transport in the field and we also observe a nonlinear signature in wavenumber domain. In this case, the theory and arguments presented above suggest that a nonlocal model of sediment transport with a nonlinear volumetric entrainment effectively characterizes the average sediment transport behavior.

4. Application: Acoustic Hillslope Experiments

To illustrate spectral behavior of land-surface evolution associated with nonlinear transport, we conducted experiments of a simulated hillslope on an acoustic table (Roering, Kirchner, Sklar, & Dietrich, 2001). This experiment generates a nonlinear particle flux with slope (Figure 5a), and we expect to observe spectral

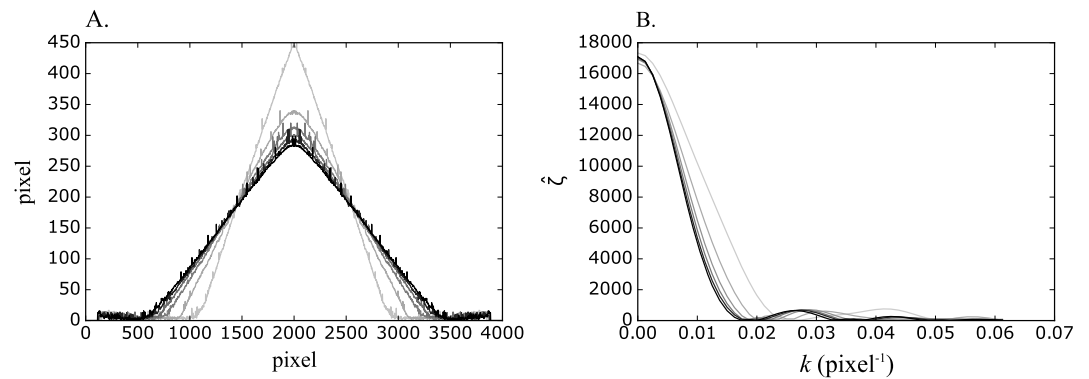


Figure 6. (a) Profiles of the surface elevation in pixels. (b) Transform of the surface elevations through time. In both plots, lighter colors correspond with older profiles. These results are from an experimental trial with intensity 2.

compression. The hillslope is a quasi-one-dimensional pile of unconsolidated spherical silica beads with relatively uniform grain size from 0.5 to 0.75 mm. The pile is constrained between two plexiglass walls that are about 15 cm apart. We sculpted an initial condition at or near the angle of repose and flanked by a long flat runoff—similar to the initial condition of a lateral moraine. The entire experiment is placed on top of a large speaker, which transmits acoustic waves of white noise through the experiment. The acoustic waves break particle force chains which allows the particles to move as a granular flow. With increasing intensity of the vibrations, the granular temperature of the particles and the active layer thickness increase, such that for a given slope, the flux increases (Furbish et al., 2008).

We track the evolution of the surface to observe the behavior of nonlinear transport processes. To do so, we placed the experiment in a dark room and highlighted the surface with a black light. Highlighting allows for a simple image analysis to determine the elevation of the surface (Figure 5). However, the light penetrates several glass bead diameters deep so a filter algorithm is not entirely smooth and produces artificial roughness. The magnitude of these artifacts are small compared to the profile, and they have negligible impact on the relevant parts of the spectra because the variance added by this noise is significantly smaller than the total variance of the landform (Figure 6). Each experiment was run until the flux became negligibly small—typically several hours.

Results from this experiment reveal that as the surface evolves, the profile maintains sharp concavities, which is consistent with a nonlinear flux formulation. In wavenumber domain, the profiles maintain the high-order structure throughout the evolution. Over the experimental time, the high-order structure consistently migrates to lower wavenumber. Observation of the evolution of this profile in configuration and wavenumber domain in concert provides an illustration of a central point of this paper. Note that in the spatial domain, the evolution of the profile is essentially elastic (Schumer et al., 2017). In wavenumber domain, basic elastic behavior is captured as the total spectral amplitude is reduced. However, for nonlinear systems, spectral amplitude migrates to lower wavenumbers to produce a smoother profile, whereas linear land-surface evolution is characterized by vertical reduction of the spectrum. Therefore, the fate of this profile is qualitatively the same as would be under linear diffusion. We argue that this is an effective illustration that linear and nonlinear processes qualitatively result in similar spatial domain evolution although they involve fundamentally different styles of spectral evolution.

5. Applications: Natural Landforms

In this section we observe spectral behavior of land-surface evolution of three different topographic configurations: a lateral moraine, a flight of river terraces, and an incised lateral moraine. We choose these configurations because they have known boundary conditions and initial conditions. In the cases of a lateral moraine and river terrace, $\zeta(\pm\infty, t) = 0$ with known initial conditions. The incised lateral moraine has a known moving boundary, which can be incorporated theoretically or numerically. We highlight that these scenarios are not necessary for the theory to be applied, but signatures of the mechanistic style of transport are only revealed when there has been some measurable topographic evolution, so a previous configuration

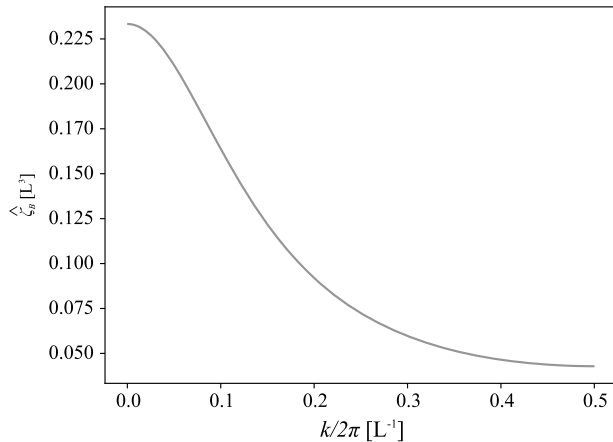


Figure 7. Power spectral density of an AR(1) process for $\sigma_\zeta^2 = 0.1$ and $\phi_B = 0.4$. Note that because it is a spectral power density, the units are L^3 . The small magnitudes suggest small magnitudes for noise in spectral amplitude.

must be known with some reasonable degree of fidelity. Topographic data from all examples were collected using either a self-leveling transit or a TruPulse Laser Range-Finder, with horizontal spacing of 1–3 m.

In natural settings, we must acknowledge that biogeomorphic processes tend to roughen the surface and therefore are expected to add spectral amplitude (Booth et al., 2017; Jyotsna & Haff, 1997). If enough variance is added to the land surface through roughness elements, then we run the risk of misinterpreting apparent added variance as a signature of non-linear processes. Before we present natural examples, we show that, so long as the landform in question is much larger than the biogeomorphic roughness, the roughness signal is negligible.

We begin with a statistical representation of topographic noise. At a horizontal resolution of a meter or less, topographic elevation at any point is likely to have a value similar to the value of points around it. We represent this idea statistically by suggesting that topographic noise is an autoregressive process of order 1, “AR(1).” Mathematically, we write this as

$$\zeta_B(j+1) = \phi_B \zeta_B(j) + w(\sigma_w^2), \quad (16)$$

where ζ_B is the land-surface elevation due to roughness, j refers to a discrete position, ϕ_B is the AR(1) parameter, and $w(\sigma_w^2)$ is white noise with variance σ_w^2 . The power spectral density of a profile generated by (16) has an analytical form (Box & Jenkins, 1976; Figure 7),

$$\hat{\zeta}_B = \frac{\sigma_\zeta^2(1 - \phi_B^2)}{1 - 2\phi_B \cos(2\pi k) + \phi_B^2}. \quad (17)$$

For the semiarid and rangeland environments considered in this paper, land-surface variance due to biogeomorphic roughness, σ_ζ^2 , is on the order of decimeters (Jyotsna & Haff, 1997), and so $\hat{\zeta}_B(k)$ is at most $\sim 1 \text{ m}^2$. Spectral amplitudes of landforms considered in this paper are much greater than 1 m^2 , and over geomorphically relevant timescales, spectral decay due to linear diffusion is much greater than the magnitude added by roughness. That is, we expect the degree of spectral decay to be much greater than 1 m^2 over timescales of 1–10 ka in most wavenumbers. Therefore, the risk of misinterpreting apparent spectral growth due to noise is minimal for relatively large and old landforms (tens of meters and kiloannum). A similar argument applies for error introduced from measurements. With this in place, we continue with natural examples and interpret any positive spectral growth rates as a result of the style of sediment transport.

5.1. Initial Conditions

The initial conditions for all landforms that we consider are assumed to be at or near angles of repose for the particular material. For glacial material this is a slope of 0.63–0.67 (Putkonen et al., 2008). We assume negligible losses to chemical weathering and a constant bulk density so that conservation of mass demands that the integrals of the initial and observed conditions are equal. These two constraints allow for a mass-conserving estimate of the initial condition.

The initial conditions are a series of planar surfaces that abruptly change slope. There is the possibility that actual initial conditions contain more rounded corners. Rounding corners, however, reduces the overall topographic variance, which, in wavenumber domain, is manifest as a reduction in spectral amplitude. Therefore, the spectral growth that is apparent in the examples below cannot be explained by errors in the initial condition. We formally show this in Appendix A.

5.2. Lateral Moraine, Bloody Canyon, CA

Lateral moraines have been the subject of several previous papers that document the degradation of topography (Doane et al., 2018; Madoff & Putkonen, 2016; Putkonen et al., 2008) because we know their initial condition and have reasonable estimates of their age. Here we focus on a lateral moraine that emerges from Bloody Canyon in the eastern Sierra Nevada. There is a suite of glacial advances recorded in the nested moraines of Bloody Canyon. However, we present the analysis for a single lateral moraine that is 40–50 ka (Kaufman et al., 2003; Phillips et al., 2009; Rood et al., 2011; Schaefer et al., 2006). The specific age of the

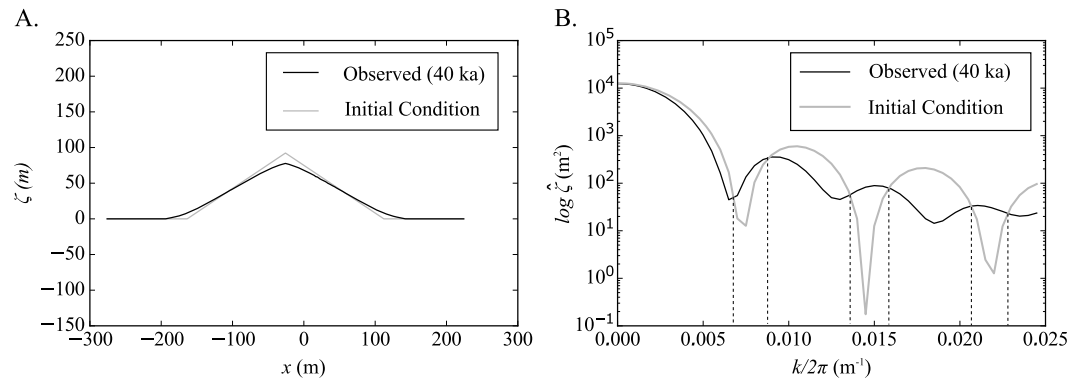


Figure 8. (a) Initial and observed profiles of a lateral moraine from Bloody Canyon, CA. (b) Transforms of initial and observed profiles. Dashed lines denote the boundary of narrow bands that have spectral growth.

moraine is unimportant for our purposes because we are simply identifying a style of evolution, not rates of evolution. The general postglacial evolution of a lateral moraine is as follows. While the glacier is active, the interior sides are supported by the glacier and are therefore oversteepened. Following recession, the side slopes rapidly adjust to the angle of repose, which for glacial till is ~ 0.67 . Meanwhile, the exterior slope remains at approximately the angle of repose during glaciation such that the initial condition is a triangle (Putkonen et al., 2008). When the glacier recedes, hillslope transport then alters the form of the moraine. Comparing the transform of the initial condition and that of the observed, we see that certain spectral bands have grown (Figure 8). The location of spectral peaks in the observed transform are offset to lower wavenumber from those in the initial spectrum. Such a behavior is consistent with the analysis for nonlinear processes.

Previous work shows that both nonlinear models like (3) and nonlocal models with nonlinear entrainment rates are capable of producing profiles that closely match the observed profiles in this location. This work identifies capacitor-style transport involving temporary storage of sediment behind shrubs and subsequent release when the shrubs die (Doane et al., 2018). In this case, the entrainment rate for nonlocal transport contains a nonlinear term, which is responsible for strong spectral compression and clear spectral growth.

5.3. Fluvial Terraces, Jackson Hole, Wyoming

The iconic terraces that flank the Snake River east of the Tetons are particularly well suited for this type of analysis (Figure 9). Since the last glacial maximum, the Snake River has incised into the glacial outwash plain (Love, 2001), leaving a series of fluvial terraces. Similar terraces have been the subject of previous



Figure 9. (a) Image of the riser between T2 and T3 on fluvial terraces near Jackson, WY. In order to highlight the terrace, the T2 is shaded in gray, and the surface of the terrace slope is highlighted in the white dashed line. (b) In certain locations, the large grains are clustered together and compose a sediment capacitor behind shrubs.

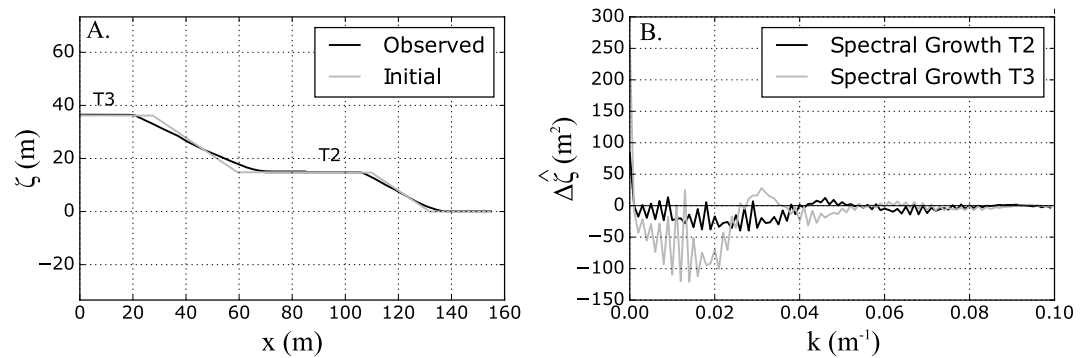


Figure 10. (a) Profile of a flight of terraces flanking the Snake River with gray profile being an idealized initial condition. (b) Spectral growth of T2 and T3 over their respective ages. Note that we have done the analysis for each terrace individually but plotted them together in their natural configuration.

work which suggests that linear diffusion does not accurately describe the evolution of fluvial terraces or fault scarps of the region (Nash & Beaujon, 2006). This work also suggests that hillslope diffusivities scale with landform size, and therefore, the flux increases with height. That the flux scales with landform size suggests that nonlocal processes are significant in this setting because longer slopes allow for greater upslope contributions to downslope fluxes with nonlocal formulations like (4).

We surveyed a flight of two terraces, T3 and T2 (Figure 10a). T3 is higher than T2 and therefore must be older and postdate Pinedale glaciation (~ 15 ka; Love, 2001). Like the moraine, these features are capable of illuminating the details of sediment transport because the initial condition is relatively well constrained. We assume an initial condition with slope of 0.65 which corresponds with the angle of repose for glacial material (Putkonen et al., 2008). On the face of terraces, boulders tend to accumulate behind shrubs. We interpret this observation as evidence of capacitor-style sediment transport, where boulders roll downslope until motion is impeded by a shrub (DiBiase & Lamb, 2013; Lamb et al., 2011, 2013). This process continues, and the area immediately upslope of the shrub gathers more boulders creating a small boulder field. The boulder field serves to capture more boulders setting up a positive feedback. If the boulder field becomes unstable by either a shrub dying or another event, then these boulders are available for transport. Larger grain sizes tend to travel further as they roll over surface roughness elements without losing as much momentum as smaller particles (DiBiase et al., 2017). Therefore, such boulder fields represent a likely source for nonlocal transport. This is just one source of nonlocality and there may be other mechanisms for long-distance transport, for example, those involving motions initiated by snow or large animals (i.e., elk, moose, and bear).

We generate spectra for each terrace individually over the same domain length. We plot change in spectral amplitude, $\Delta\hat{\zeta} = |\hat{\zeta}_T| - |\hat{\zeta}_0|$ (Figure 10b) where subscripts T and 0 refer to observed and initial transforms, respectively. The use of the magnitudes of spectral amplitudes here does not change the signature of linear or nonlinear processes. Linear processes will always result in reduction of the magnitude of spectral amplitudes, whether or not they are positive or negative in the amplitude spectrum. Therefore, positive change in the spectrum indicates compression and nonlinear processes. There is more growth in T3; however, T2 also shows definitive growth. Wavenumbers that grow correspond with the width of the terrace riser and its harmonics. We interpret this as spectral growth as opposed to a red noise signal because the spectral amplitude is larger than what we expect from a reasonable estimate of the noise (0.1 m^2) in this setting and because the $\Delta\hat{\zeta}$ does not share a similar form expected for a red noise. Spectral growth in this style is consistent with the style from moraine evolution and suggests that sediment transport contains a nonlinearity with slope. Given the evidence for nonlocal transport by temporary storage and release of boulders among other nonlocal processes, we suggest that a nonlinearity with respect to slope is present in the volumetric entrainment rate.

5.4. Incision Into a Plain

The two previous examples represent topographic configurations that lack a channel boundary. In order to explore the impact of a moving boundary condition, we consider a plain that is incised by a channel. Let us suggest that the channel incises at a uniform rate. Mathematically, we represent incision as a unit step function of magnitude v [L T^{-1}], which has a transform that is a uniform function with value v (Poularikas,

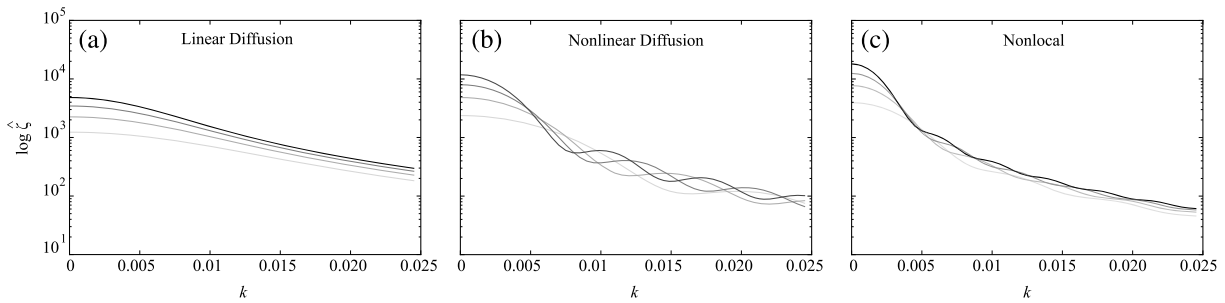


Figure 11. Amplitude spectra of land-surface elevation from numerical models simulating channel incision and hillslope relaxation for linear (a), nonlinear (b), and nonlocal (c) models. The older profiles correspond to lighter colors. Field data of untransformed profiles for this scenario are presented in Figure 13a.

1998). In the absence of hillslope processes, pure incision would cut a canyon with vertical walls, whose transform is a uniform function with value vT , where T is the duration of incision. Adding hillslope processes to this scenario relaxes the side slopes and alters the uniform transform. The style in which side slopes relax according to linear and nonlinear transport are expected to be different and highlighted in wavenumber domain.

We begin with linear diffusion. With reference to (9), we note that over every interval of time for which $v\Delta t$ is added to the spectrum by pure incision, this signal is counteracted by linear diffusion, which retards the growth of the spectrum at high wavenumbers. In this case, the boundary condition adds variance to the land-surface, which adds spectral amplitude and spectral growth is *not* a signature of nonlinear processes. We instead look for a signature in the form of the transform. The evolution of the spectrum is

$$\hat{\zeta}_t(k) = v\Delta t - k^2 D (v\Delta t + \hat{\zeta}(k)) . \quad (18)$$

Consider the initial incision into a plain. After Δt , the transform of the land surface is

$$\hat{\zeta}(k, \Delta t) = v\Delta t (1 - k^2 D) , \quad (19)$$

which is a monotonically decreasing function of k . With continued evolution, this basic form remains, but the magnitude changes. We are not aware of an analytical solution for the spectrum of the land surface through time for any of the models and so we numerically simulate this configuration for all models to explore their behavior.

The initial condition is a flat surface with boundary conditions $\frac{dz}{dt}(0, t) = -v$ and $\zeta(\infty, t) = 0$. In all cases, continued land-surface evolution leads to transforms that share the low-order structure. That is, broadly, all spectra decay approximately exponentially with k . However, elevation spectra for nonlinear and nonlinear nonlocal models have a periodic signal that changes the high-order structure (Figures 11b and 11c). In summary, for this boundary condition, spectra of land-surface profiles evolving according to linear diffusion contain no harmonics, whereas those evolving according to nonlinear processes do contain harmonics. We

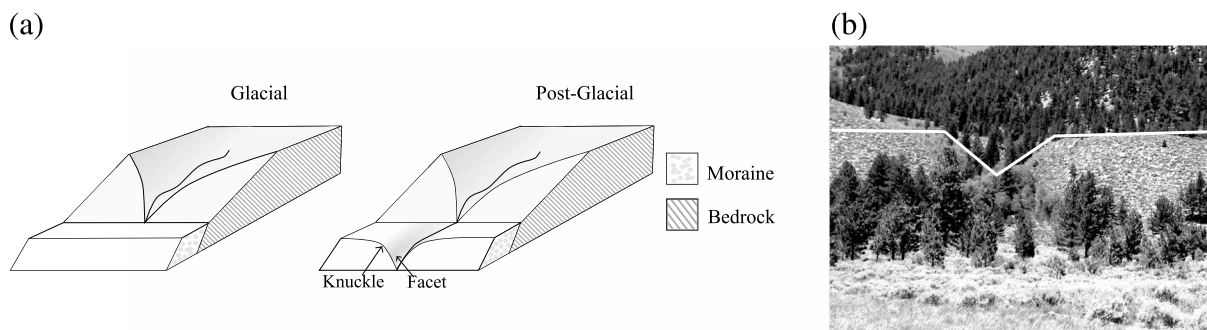


Figure 12. (a) Block diagram showing the evolution of a butressed moraine. The facet is the surface that forms from postglacial incision through the lateral moraine. The knuckle of the facet is the location at the top of the slope where the surface rolls over to horizontal. (b) Photograph of the facet surveyed at Twin Lakes, CA. The white line outlines the land surface. In both figures, the moraine is 50 m tall.

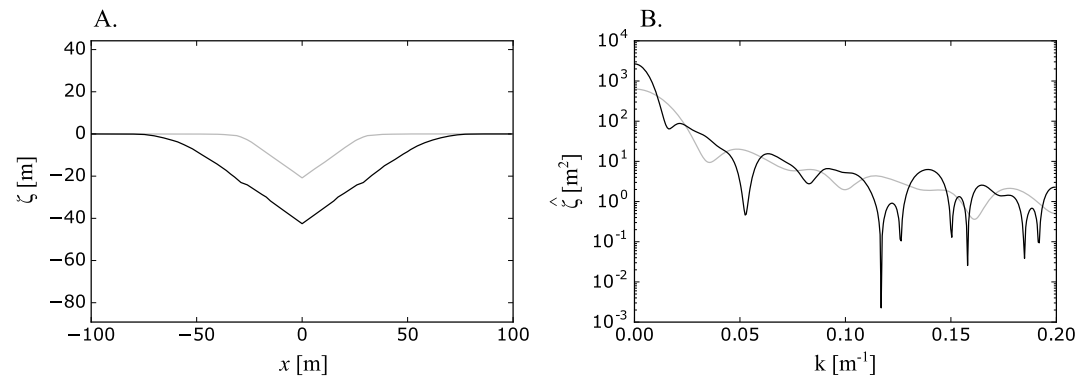


Figure 13. (a) Land-surface profiles of incised moraine. (b) Fourier transforms of profiles. Line colors correlate between (a) and (b). Note the semiperiodic structure of the spectra that is present, suggesting a nonlinearity in the transport process. Refer for Figure 11 for the behaviors associated with different models.

emphasize that the presence of harmonics are only a signature of nonlinearity for this boundary condition. In configuration space, the high-order structure reflects the relatively sharp concavity that is maintained at the knuckle of the facet (Figure 12).

We apply this idea to a natural example which is a buttressed lateral moraine near Twin Lakes, CA. The moraine is last glacial maximum age (Rood et al., 2011), and we suggest that the moraine has been incised since deposition. Our conceptual model of the evolution of this features is as follows. While the glacier is active, the lateral moraine is buttressed by the valley walls and sediment is supplied by the hillslope and the active glacier such that the lateral moraine becomes a flat bench (Figure 12a). When the glacier recedes, sediment supply diminishes and the extant channel can begin to incise through the flat moraine (Figure 12b). As incision continues, hillslope processes act on the facet that is created and the facet geometry reflects the mechanics of sediment transport. Incision begins at the edge of the bench, where it drops to the valley floor, and works back to the extant channel. As such, the portion of the facet nearest the valley has the longest incision history. We surveyed two profiles along one facet, one close to the edge of the bench and one closer to the buttressing hillslope. The profiles are of different lengths and have been associated with active incision for different time spans or rates.

Profiles along a facet of the incised moraine are relatively straight and high concavity characterizes the knuckle of the facet (Figure 13a). In wavenumber domain, both profiles exhibit a nonmonotonically decreasing spectra with quasiperiodic peaks and troughs. Such behavior is mirrored in nonlinear simulations of this scenario where the spectrum is a decaying periodic function with k (Figure 11). In our natural example, we observe strongly nonlinear behavior with the spectrum periodically approaching zero (Figure 13b). The higher-order structure contained in this transform reflects the high concavity contained in the knuckle of the facet and is a signature of nonlinear transport. In this case, field evidence for nonlocal transport is not readily evident although it is likely that nonlocal processes occur here as they do for the example of the lateral moraine.

6. Discussion

6.1. Two End-Members for the Destruction of Variance

At this point, we consider two fundamentally different paths by which the land surface can evolve—straightening and lengthening. Straightening refers to rounding sharp concavities, which tends to degrade topographic highs and fill in hollows for conditions that lack external control on the boundary conditions (channel incision, uplift). Lengthening implies that topographic forms become wider but meanwhile maintain sharp concavity. Lengthening is akin to slope replacement. To be clear, both methods result in a landform becoming wider as sediment is deposited at positive concavities for linear and nonlinear models. If the difference between these terms appears subtle, that is because the physical manifestations between different transport models is subtle. We use these terms here as we define and explore two fundamentally different styles that become clearer when viewed in wavenumber domain. Both methods are mass conserving and result in a reduction of topographic variance. As such, they are reasonable descriptions of topographic evolution. We associate straightening with linear diffusion, as it effectively diminishes sharp concavities. On

observation of Figures 8a and 6a, we note that nonlinear processes are effective at lengthening topographic forms. With these distinctions in place, we question which topographic forms display nonlinear behavior and which ones might obscure it.

In the examples presented above, topographic lengthening in the spatial domain is represented by compression in wavenumber domain. For illustration, consider the transform of a triangle,

$$\hat{\xi} = LH \left(\frac{\sin(\frac{kL}{2})}{\frac{kL}{2}} \right)^2, \quad (20)$$

where L [L] is one half the triangle width and H [L] is the triangle height. When a triangle is stretched in a mass-conserving way, the lengthening is accommodated by a reduction in H . In the wavenumber domain, this results in a translation of the transform to lower wavenumbers. We mathematically describe compression as advection to lower wavenumbers; however, to maintain periodicity, the magnitude of advection, c , must increase linearly such that $c(k) = -\gamma k$, where γ [T⁻¹] is a rate constant related to the rate of stretching (Appendix B).

Imagine a triangle that is lengthened by increasing L and decreasing H . Conservation of mass demands that $A = HL$ remains constant as stretching occurs. Placing $c(k)$ into an advection equation,

$$\frac{\partial \hat{\xi}}{\partial t} = -\gamma k \frac{\partial \hat{\xi}}{\partial k} + W(k), \quad (21)$$

where $W(k)$ is a sink term. We use Leibniz notation for derivatives here to be consistent with typical representation of advection equations. Insofar as topographic stretching results from nonlinear transport processes, we suggest that the advective component of (21) results from the nonlinear transport and $W(k)$ represents the loss of spectral amplitude due to linear diffusion,

$$W(k) = -k^2 D \hat{\xi}. \quad (22)$$

Recall that a nonlinear formulation for sediment transport contains a linear term as in (11) so this formulation can effectively represent a nonlinear model in wavenumber domain. We note that spectral compression is only a kinematic description of the evolution of the spectra and is a simplification of the actual process. However, casting nonlinear systems this way provides a simple way to investigate which topographic configurations highlight distinctive behaviors between linear and nonlinear processes.

We suggest that a combination of topographic stretching (spectral compression) and straightening (spectral decay) that corresponds with the relative magnitude of nonlinear and linear processes accounts for landform evolution. However, because the first-order control on sediment transport is slope, the rate of stretching must decline as slope reduces. We add a modulating term, $m(t)$ to c (Appendix B), which is a dimensionless coefficient that relates the dependency of c to the land-surface slope. We represent the impact of m by plotting the rates of spectral advection (stretching), $c(k, t)$, with that of vertical spectral decay (straightening), $W(k)$. With continued evolution, the magnitude of spectral celerity continues to reduce, whereas the diffusivity for linear diffusion remains constant and so does the ability to destroy topographic variance (Figure 14). Therefore, certain topographic configurations may initially exhibit nonlinear behavior that gives way to linear diffusion. Previous work highlights this pattern in numerical simulations of an evolving moraine (Doane et al., 2018), where early spectral growth is rapid and contained in high wavenumbers but gives way to slower growth rates in lower wavenumbers. Eventually, spectral compression becomes negligible and appears to be almost entirely driven by spectral decay—although perhaps not exactly in the same manner as linear diffusion (Doane et al., 2018).

Certain topographic configurations are likely to exhibit nonlinear behavior more clearly than others. We have identified that positive spectral growth can be a signature of nonlinear processes. This occurs because nonlinear processes drive compression in the wavenumber domain. Therefore, any spectra with a positive gradient with respect to k will temporarily grow as spectral amplitude is advected toward the origin. A positive gradient in wavenumber domain often implies a spectra that contains finite amplitude in its high-order structure, which typically reflects sharp concavities in the spatial domain. Most topographic features for which we have reasonable estimates of the initial condition contain sharp concavities (i.e., lateral moraines,

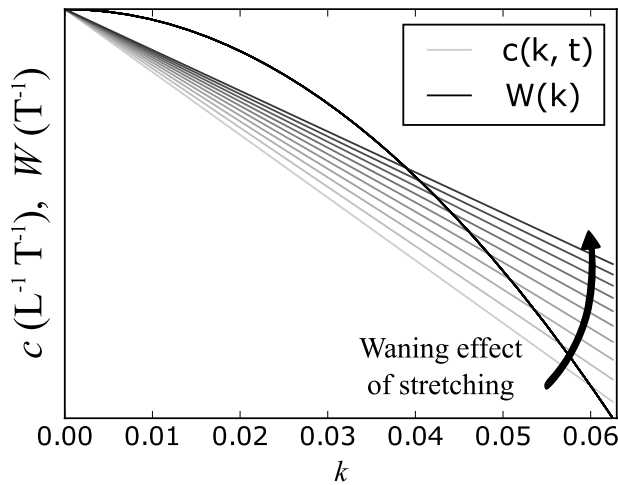


Figure 14. Spectral celerity from nonlinear processes (grayscale lines) and spectral decay rates from linear diffusion through time. Although not directly comparable due to different units, the spectral celerity, c , decays with time whereas the rate constant associated with spectral decay for linear diffusion remains constant. Lighter lines represent celerities at earlier times in topographic evolution.

terraces, and incised plains), and therefore, these features are effective tools for identifying the style of sediment transport that drives topographic evolution.

Whereas certain topographic configurations will highlight nonlinear and nonlocal transport, there are others that may obscure such behavior in wavenumber domain. If nonlinear processes are most clearly observed in spectra that have positive gradients with respect to k , then those that lack positive gradients will not highlight nonlinear processes. For configurations lacking channel boundaries, spectra with only negative gradients can only show spectral decay by both nonlinear and linear diffusion, obscuring the distinguishing behavior. To be clear, spectra with only negative gradients may still evolve differently according to the three transport models, but the differences will be subtle. A spectrum for which nonlinear behavior is completely matched by linear diffusion does exist. By rearranging (21) to set the advection and sink terms equal to each other

$$-Dk^2\hat{\zeta} = \gamma k \frac{d\hat{\zeta}}{dk}. \quad (23)$$

Separating variables and integrating then reveals that a spectrum with a form

$$\hat{\zeta}(k) = e^{-\frac{Dk^2}{2\gamma}} \quad (24)$$

will momentarily evolve identically according to linear and nonlinear processes. The inverse transform of (24) is itself a Gaussian function and the land-surface profile is

$$\zeta(x) = \sqrt{\frac{\gamma}{D}} e^{-\frac{\gamma x^2}{2D}}. \quad (25)$$

In contrast to triangles or terraces, Gaussian functions effectively distribute concavity over the entire function such that no single point is characterized by large concavity values. Although the form presented in (25) completely obscures the distinction between nonlinear and linear diffusion, forms that share the characteristic of having relatively small concavity will effectively obscure diagnostic behavior as well. We emphasize that this analysis highlights the importance of the initial condition for *observation* of signatures of the mechanistic style of sediment transport, it does not invalidate any of the theory presented in section 2. That is, land-surface evolution in wavenumber domain will still evolve by spectral compression or decay, but those two will look increasingly similar for land surfaces that are close to Gaussian in form. This observation leads us to consider Gaussian hillslopes in refining a definition of low-order structure.

Consider fitting the Gaussian hillslope with a simple triangle such that the mismatch between the two is minimized. We note that there is a clear mismatch; however, a triangle can explain much of the variance of a Gaussian profile (Figure 15a). That the two functions largely share how variance is distributed illustrates what we mean by low-order structure. This becomes particularly clear when the functions are viewed in wavenumber domain. The transforms of both the Gaussian and triangle are similar at low wavenumber, and the spectral amplitude within this low wavenumber band makes up most of the variance. However, distinct differences are observed in the high wavenumbers, which highlight the high-order structure. Whereas the bulk of the variance is contained in the low-order structure of the land-surface profile, there is a disproportionate amount of information contained in the high-order structure, which is the difference between a Gaussian and a triangle (Figure 15b). Here we emphasize an important point. We note that the transform of a Gaussian contains vanishingly small amplitude in its high-order structure. This is not to say that it does not have high-order structure, but that the infinitesimal amplitudes are a signature of the Gaussian form.

We can further explore the significance of Gaussian forms. Insofar as we can suggest that sediment transport is slope dependent, then linear diffusion is a first-order description of land-surface evolution. Gaussian profiles have the unique property that the functional form remains the same throughout evolution according to linear diffusion. An initial Gaussian form remains a Gaussian during diffusion, but the amplitude is

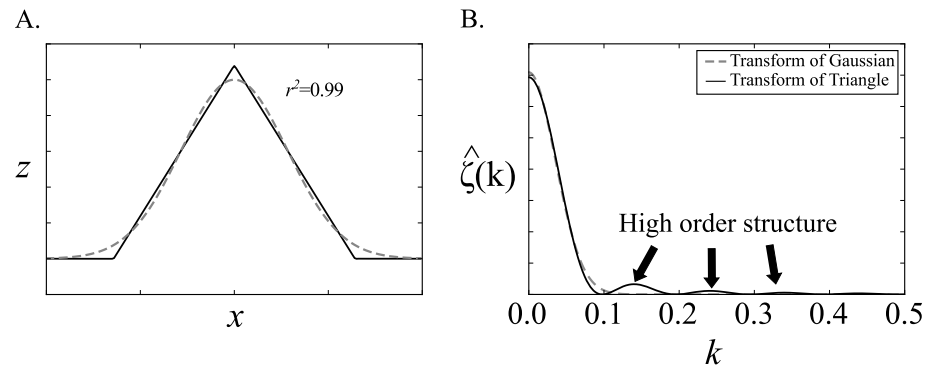


Figure 15. Illustration of the similarities and differences between a Gaussian and a triangle (a), which, despite obvious differences, share a low-order structure that is apparent in the spectrum of the two functions (b).

reduced. Therefore, although a rigid definition for low-order structure is difficult to determine, we suggest that the best fit Gaussian form is the low-order structure for a given landform. The high-order structure then is contained in the part of the spectrum that deviates from that Gaussian form, which for most isolated landforms like a moraine represents a relatively small part of the topographic variance. The evolution of that high-order structure contains the clues to the mechanistic style of sediment transport. This is a working definition and there are perhaps other equally satisfying definitions.

7. Conclusion

We have shown that linear and nonlinear processes are associated with different spectral behaviors for certain topographic configurations with specified boundary conditions. Linear diffusion unambiguously shows spectral decay in every wavenumber. Nonlinear diffusion drives a compression of the spectrum to lower wavenumbers, which can result in growing spectral amplitudes for certain topographic configurations. Non-local transport can display linear or nonlinear behavior—depending on the form of the entrainment rate. The effect of the probability function of travel distance, however, is to modify the linear or nonlinear behavior (Figure 2), although it may be subtle. For example, the evolution of a hillslope formed by incision into a plain shows similar spectral evolution for nonlinear diffusion and nonlocal transport (Figure 11).

These signatures are readily distinguished for land-surface configurations that have an initial or previously known condition that has positive gradients in wavenumber domain. If this condition is satisfied then signatures will be observable in the difference between the transforms of the initial and observed landform. We recognize we can only know this for a small portion of the landscape, but if such a feature can be identified, the mechanistic style may be applicable to the entire region. For example, even in the quasi-steady state landscape of the Oregon Coast Range, there are fluvial terraces preserved (Almond et al., 2007), which may offer some clues to the mechanistic style of sediment transport. Furthermore, whereas concavity can be used to identify nonlinear versus linear diffusion in steady state hillslopes, the spectral signature is applicable to transient scenarios.

We have demonstrated that the three common transport models are elastic (Schumer et al., 2017) as they contain slope as a central ingredient. As such, they tend to degrade topography and, in the absence of tectonic forcing, the land-surface evolves toward zero variance. In wavenumber domain, we see that there are two distinct ways to do this. Linear diffusion drives a vertical variance destruction, which decays spectral amplitude in place. Nonlinear processes tend to compress all of the variance into consistently lower wavenumbers. Ultimately, when all spectral amplitude is contained in the zero wavenumber, the land surface has reached zero variance.

Appendix A: Initial Condition

We recognize that the initial conditions for landforms may contain rounded knuckles, whereas we have used sharp boundaries. We show here that more rounded initial conditions cannot result in the observed bands of spectral growth for the landforms used in this paper. To do so, we imagine smoothing our chosen initial conditions.

A common method of smoothing a function is by implementing a moving average. Such an operation is a convolution of the function with a weighting function—which is commonly a Gaussian function that integrates to unity. The transform of this Gaussian is itself a Gaussian. A convolution in the spatial domain is multiplication in wavenumber domain so a smoothed initial condition would be

$$\hat{\zeta}_i(k) = a\hat{\zeta}(k, 0)e^{-l^2k^2}, \quad (\text{A1})$$

where l is a characteristic length of the averaging window and a is the amplitude of the transform of the weighting function. The transform of the smoothing window is everywhere less than one, so the only possibility is for spectral amplitudes to be less than an initial condition with sharp corners and thus spectral growth is not attributable to more rounded initial conditions.

Appendix B: Rate of Spectral Compression as a Function of Time and k

Here we illustrate that compressing a spectral function, as related to stretching in the spatial domain, can be accomplished by advection with a linearly varying celerity. We illustrate this with an example of spectral compression of a triangle. The transform of a triangle is

$$\hat{\zeta}(k) = HL \left[\frac{\sin(kL/2)}{kL/2} \right]^2, \quad (\text{B1})$$

where H is height and L is the half width. Note that stretching (B1) in a mass-conserving way demands that as L lengthens H decreases such that $A = HL$ remains constant. Lengthening is represented by

$$\frac{\partial \hat{\zeta}}{\partial t} = \frac{\partial \hat{\zeta}}{\partial L} \frac{dL}{dt}. \quad (\text{B2})$$

The derivative with respect to L ,

$$\frac{d\hat{\zeta}}{dL} = 2A \left[\frac{\sin(kL/2)}{kL/2} \right] \left[\frac{\frac{k^2L}{4} \cos(kL/2) - \frac{2L}{4} \sin(kL/2)}{(kL/2)^2} \right], \quad (\text{B3})$$

and we specify $\frac{dL}{dt} = m$. According to the advection equation,

$$\frac{\partial \hat{\zeta}}{\partial L} \frac{dL}{dt} = -c(k) \frac{\partial \hat{\zeta}}{\partial k}, \quad (\text{B4})$$

where $c(k)$ is a spectral celerity ($L^{-1} T^{-1}$). The derivative with respect to k

$$\frac{d\hat{\zeta}}{dk} = 2A \left[\frac{\sin(kL/2)}{kL/2} \right] \left[\frac{\frac{kL^2}{4} \cos(kL/2) - \frac{2k}{4} \sin(kL/2)}{(kL/2)^2} \right]. \quad (\text{B5})$$

Solving for $c(k)$

$$c(k) = -m \left[\frac{k^2L \cos(kL/2) - 2k \sin(kL/2)}{kL^2 \cos(kL/2) - 2L \sin(kL/2)} \right] = -m \frac{k}{L}, \quad (\text{B6})$$

which, despite the form, is a linear function of k . We can also relate γ from equations (21)–(25) to $c(k)$ and discover that $\gamma = \frac{m}{L}$ in this case.

As written, (B6) describes the spectral evolution of a triangle that stretches by a constant dL/dt . We heuristically imagine that the rate of stretching scales with slope, H/L . If we specify that $\frac{dL}{dt} = m \frac{H}{L}$, we can solve for $L(t)$,

$$\frac{dL}{dt} = m \frac{H}{L} = m \frac{A}{L^2}. \quad (\text{B7})$$

Separating variables and integrating

$$L(t) = (3mAt)^{1/3} + L_0, \quad (\text{B8})$$

where L_0 [L] is an initial length. Note that although we suggest the rate of stretching varies linearly with slope, this does not suggest that the flux varies linearly with slope. Indeed the slope dependency of stretching could be nonlinear where

$$\frac{dL}{dt} = m \left[\frac{H}{L} \right]^\beta, \quad (\text{B9})$$

which leads to

$$L(t) = [(2\beta + 1)mA^\beta t]^{(\frac{1}{2\beta+1})} + L_0 \quad (\text{B10})$$

and is valid for $\beta > 0$. In these cases, $c(k, L)$, such that the advective velocity decreases with time. As $\beta \rightarrow 0$, the rate of stretching becomes increasingly insensitive to the slope.

Acknowledgments

We acknowledge support by the National Science Foundation (EAR-1625311 to D. L. R., EAR-1420831 to D. J. F., and EAR-1420898 to J. J. R.). Topographic data sets, photos from the acoustic experiment, and Python codes for analysis are available for download at <https://ir.vanderbilt.edu/handle/1803/9343>. We thank two anonymous reviewers who provided thoughtful feedback that strengthened the manuscript. We thank Brandon McElroy for generously providing field equipment and Daniel Morgan, Timothy Watkins, Sarah Sams, and Aiden and Jesse Emilo for assistance in the field.

References

- Almond, P., Roering, J. J., & Hales, T. C. (2007). Using soil residence time to delineate spatial and temporal patterns of transient landscape response. *Journal of Geophysical Research*, *112*, F03S17. <https://doi.org/10.1029/2006JF000568>
- Booth, A. M., LaHusen, S. R., Duvall, A. R., & Montgomery, D. R. (2017). Holocene history of deep-seated landsliding in the North Fork Stillaguamish River valley from surface roughness analysis, radiocarbon dating, and numerical landscape evolution modeling. *Journal of Geophysical Research: Earth Surface*, *122*, 456–472. <https://doi.org/10.1002/2016JF003934>
- Box, G. E., & Jenkins, G. M. (1976). *Time series analysis: Forecasting and control*. San Francisco, CA: Holden-Day.
- Carslaw, H. S., & Jaeger, J. C. (1959). *Conduction of heat in solids* (2nd ed.). Oxford: Clarendon Press.
- Carson, M. A., & Kirkby, M. J. (1972). Hillslope form and process, 475.
- Culling, W. (1963). Soil creep and the development of hillside slopes. *Journal of Geology*, *71*(2), 127–161.
- Culling, W. (1965). Theory of erosion on soil-covered slopes. *The Journal of Geology*, *73*, 230–254.
- DiBiase, R. A., & Lamb, M. P. (2013). Vegetation and wildfire controls on sediment yield in bedrock landscapes. *Geophysical Research Letters*, *40*, 1093–1097. <https://doi.org/10.1002/grl.50277>
- DiBiase, R. A., Lamb, M. P., Ganti, V., & Booth, A. M. (2017). Slope, grain size, and roughness controls on dry sediment transport and storage on steep hillslopes. *Journal of Geophysical Research: Earth Surface*, *122*, 941–960. <https://doi.org/10.1002/2016JF003970>
- DiBiase, R. A., Whipple, K. X., Heimsath, A. M., & Ouimet, W. B. (2010). Landscape form and millennial erosion rates in the San Gabriel Mountains, CA. *Earth and Planetary Science Letters*, *289*(1), 134–144. <https://doi.org/10.1016/j.epsl.2009.10.036>
- Doane, T. H., Furbish, D. J., Roering, J. J., Schumer, R., & Morgan, D. J. (2018). Nonlocal sediment transport on steep lateral moraines, eastern Sierra Nevada, California, USA. *Journal of Geophysical Research: Earth Surface*, *123*, 187–208. <https://doi.org/10.1002/2017JF004325>
- Fernandes, N. F., & Dietrich, W. E. (1997). Hillslope evolution by diffusive processes: The timescale for equilibrium adjustments. *Water Resources Research*, *33*(6), 1307–1318. <https://doi.org/10.1029/97WR00534>
- Foufoula-Georgiou, E., Ganti, V., & Dietrich, W. (2010). A nonlocal theory of sediment transport on hillslopes. *Journal of Geophysical Research*, *115*, F00A16. <https://doi.org/10.1029/2009JF001280>
- Furbish, D. J., Childs, E. M., Haff, P. K., & Schmeekle, M. W. (2009). Rain splash of soil grains as a stochastic advection-dispersion process, with implications for desert plant-soil interactions and land-surface evolution. *Journal of Geophysical Research*, *114*, F00A03. <https://doi.org/10.1029/2009JF001265>
- Furbish, D. J., & Fagherazzi, S. (2001). Stability of creeping soil and implications for hillslope evolution. *Water Resources Research*, *37*(10), 2607–2618. <https://doi.org/10.1029/2001WR000239>
- Furbish, D. J., & Haff, P. K. (2010). From divots to swales: Hillslope sediment transport across diverse length scales. *Journal of Geophysical Research*, *115*, F03001. <https://doi.org/10.1029/2009JF001576>
- Furbish, D. J., Haff, P. K., & Dietrich, W. E. (2009). Statistical description of slope-dependent soil transport and the diffusion-like coefficient. *F00A05*, *114*. <https://doi.org/10.1029/2009JF001267>
- Furbish, D. J., & Roering, J. J. (2013). Sediment disentrainment and the concept of local versus nonlocal transport on hillslopes. *Journal of Geophysical Research: Solid Earth*, *118*, 937–952. <https://doi.org/10.1002/jgrf.20071>
- Furbish, D. J., Schmeekle, M. W., & Roering, J. J. (2008). Thermal and force-chain effects in an experimental, sloping granular shear flow. *Earth Surface Process and Landforms*, *33*, 2108–2117. <https://doi.org/10.1002/esp.1655>
- Gabet, E. J. (2000). Gopher bioturbation: Field evidence for non-linear hillslope diffusion. *Earth Surface Processes and Landforms*, *25*(13), 1419–1428.
- Gabet, E. J. (2003). Sediment transport by dry ravel. *Journal of Geophysical Research*, *108*(B1), 2049. <https://doi.org/10.1029/2001JB001686>
- Gabet, E. J., & Mendoza, M. K. (2012). Particle transport over rough hillslope surfaces by dry ravel: Experiments and simulations with implications for nonlocal sediment flux. *Journal of Geophysical Research*, *117*, F03014. <https://doi.org/10.1029/2011JF002229>
- Ganti, V., Meerschaert, M. M., Foufoula-Georgiou, E., Virapelli, E., & Parker, G. (2010). Normal and anomalous diffusion of gravel tracer particles in rivers. *Journal of Geophysical Research*, *115*, F00A12. <https://doi.org/10.1029/2008JF001222>
- Ganti, V., Passalacqua, P., & Foufoula-Georgiou, E. (2012). A sub-grid scale closure for nonlinear hillslope sediment transport models. *Journal of Geophysical Research*, *117*, F02012. <https://doi.org/10.1029/2011JF002181>
- Gilad, E., & von Hardenberg, J. (2006). A fast algorithm for convolution integrals with space and time variant kernels. *Journal of Computational Physics*, *216*, 326–336. <https://doi.org/10.1016/j.jcp.2005.12.003>
- Hales, T., Scharer, K., & Wooten, R. (2012). Southern appalachian hillslope erosion rates measured by soil and detrital radiocarbon in hollows. *Geomorphology*, *138*(1), 121–129. <https://doi.org/10.1016/j.geomorph.2011.08.030>
- Hornberger, G., & Wiberg, P. (2013). *Numerical Methods in the Hydrological Sciences*. American Geophysical Union. <https://doi.org/10.1002/9781118709528.ch8>
- Hughes, M. W., Almond, P. C., & Roering, J. J. (2009). Increased sediment transport via bioturbation at the last glacial-interglacial transition. *Geology*, *37*(10), 919–922.
- Hurst, M. D., Mudd, S. M., Walcott, R., Attal, M., & Yoo, K. (2012). Using hilltop curvature to derive the spatial distribution of erosion rates. *Journal of Geophysical Research*, *117*, F02017. <https://doi.org/10.1029/2011JF002057>

- Jyotsna, R., & Haff, P. K. (1997). Microtopography as an indicator of modern hillslope diffusivity in arid terrain. *Geology*, *25*(8), 695–698. [https://doi.org/10.1130/0091-7613\(1997\)025<0695:MAAIOM>2.3.CO;2](https://doi.org/10.1130/0091-7613(1997)025<0695:MAAIOM>2.3.CO;2)
- Kaufman, D. S., Porter, S. C., & Gillespie, A. R. (2003). Quaternary alpine glaciation in Alaska, the Pacific northwest, Sierra Nevada, and Hawaii. *Developments in Quaternary Science*, *1*, 77–103. [https://doi.org/10.1016/S1571-0866\(03\)01005-4](https://doi.org/10.1016/S1571-0866(03)01005-4)
- Kirkby, M., & Statham, I. (1975). Surface stone movement and scree formation. *The Journal of Geology*, *83*(3), 349–362. <https://doi.org/10.1086/628097>
- Lamb, M. P., Levina, M., DiBiase, R. A., & Fuller, B. M. (2013). Sediment storage by vegetation in steep bedrock landscapes: Theory, experiments, and implications for postfire sediment yield. *Journal of Geophysical Research: Earth Surface*, *118*, 1147–1160. <https://doi.org/10.1002/jgrf.20058>
- Lamb, M. P., Scheingross, J. S., Amidon, W. H., Swanson, E., & Limaye, A. (2011). A model for fire-induced sediment yield by dry ravel in steep landscapes. *Journal of Geophysical Research*, *116*, F03006. <https://doi.org/10.1029/2010JF001878>
- Love, J. (2001). *Geologic map of the Moose Quadrangle, Teton County, WY*. USA: Wyoming State Geological Survey.
- Madoff, R. D., & Putkonen, P. (2016). Climate and hillslope degradation vary in concert; 85ka to present, eastern Sierra Nevada, CA, USA. *Geomorphology*, *266*, 33–40. <https://doi.org/10.1016/j.geomorph.2016.05.010>
- McGuire, L. A., Pelletier, J. D., & Roering, J. J. (2014). Development of topographic asymmetry: Insights from dated cinder cones in the western United States. *Journal of Geophysical Research: Earth Surface*, *119*, 1725–1750. <https://doi.org/10.1002/2014JF003081>
- Mudd, S. M., & Furbish, D. J. (2007). Responses of soil-mantled hillslopes to transient channel incision rates. *Journal of Geophysical Research*, *112*, F03S18. <https://doi.org/10.1029/2006JF000516>
- Nash, D. B., & Beaujon, J. S. (2006). Modeling degradation of terrace scarps in Grand Teton National Park, USA. *Geomorphology*, *75*(3), 400–407. <https://doi.org/10.1016/j.geomorph.2005.07.027>
- Perron, J. T., Kirchner, J. W., & Dietrich, W. E. (2008). Spectral signatures of characteristic spatial scales and nonfractal structure in landscapes. *Journal of Geophysical Research*, *113*, F04003. <https://doi.org/10.1029/2007JF000866>
- Perron, J. T., Richardson, P. W., Ferrier, K. L., & Lap tre, M. (2012). The root of branching river networks. *Nature*, *492*(7427), 100–103. <https://doi.org/10.1038/nature11672>
- Phillips, F. M., Zreda, M., Plummer, M. A., Elmore, D., & Clark, D. H. (2009). Glacial geology and chronology of bishop creek and vicinity, eastern Sierra Nevada, California. *Geological Society of America Bulletin*, *121*(7-8), 1013–1033. <https://doi.org/10.1130/B26271.1>
- Poularikas, A. D. (1998). *Handbook of formulas and tables for signal processing* (Vol. 13). Verlag Berlin Heidelberg: CRC Press.
- Putkonen, J., Connolly, J., & Orloff, T. (2008). Landscape evolution degrades the geologic signature of past glaciations. *Geomorphology*, *97*(1), 208–217. <https://doi.org/10.1016/j.geomorph.2007.02.043>
- Reneau, S. L., & Dietrich, W. E. (1991). Erosion rates in the southern Oregon Coast Range: Evidence for an equilibrium between hillslope erosion and sediment yield. *Earth Surface Processes and Landforms*, *16*(4), 307–322. <https://doi.org/10.1002/esp.3290160405>
- Roering, J. J., Kirchner, J. W., & Dietrich, W. E. (1999). Evidence for nonlinear, diffusive sediment transport on hillslopes and implications for landscape morphology. *Water Resources Research*, *35*(3), 853–870. <https://doi.org/10.1029/1998WR900090>
- Roering, J. J., Kirchner, J. W., & Dietrich, W. E. (2001). Hillslope evolution by nonlinear, slope-dependent transport: Steady state morphology and equilibrium adjustment timescales. *Journal of Geophysical Research*, *106*, 499–513. <https://doi.org/10.1029/2001JB000323>
- Roering, J. J., Kirchner, J. W., Sklar, L. S., & Dietrich, W. E. (2001). Hillslope evolution by nonlinear creep and landsliding: An experimental study. *Geology*, *29*(2), 143–146. [https://doi.org/10.1130/0091-7613\(2001\)029<0143:HEBNCA>2.0.CO;2](https://doi.org/10.1130/0091-7613(2001)029<0143:HEBNCA>2.0.CO;2)
- Roering, J. J., Perron, J. T., & Kirchner, J. W. (2007). Functional relationships between denudation and hillslope form and relief. *Earth and Planetary Science Letters*, *264*(1), 245–258. <https://doi.org/10.1016/j.epsl.2007.09.035>
- Rood, D. H., Burbank, D. W., & Finkel, R. C. (2011). Chronology of glaciations in the Sierra Nevada, California, from 10Be surface exposure dating. *Quaternary Science Reviews*, *30*(5), 646–661. <https://doi.org/10.1016/j.quascirev.2010.12.001>
- Schaefer, J. M., Denton, G. H., Barrell, D. J., Ivy-Ochs, S., Kubik, P. W., Andersen, B. G., et al. (2006). Near-synchronous interhemispheric termination of the last glacial maximum in mid-latitudes. *Science*, *312*(5779), 1510–1513. <https://doi.org/10.1126/science.1122872>
- Schumer, R., Meerschaert, M. M., & Baeumer, B. (2009). Fractional advection-dispersion equations for modeling transport at the Earth surface. *Journal of Geophysical Research*, *114*, F00A07. <https://doi.org/10.1029/2008JF001246>
- Schumer, R., Taloni, A., & Furbish, D. J. (2017). Theory connecting nonlocal sediment transport, Earth surface roughness, and the Sadler effect. *Geophysical Research Letters*, *44*, 2281–2289. <https://doi.org/10.1002/2016GL072134>
- Tucker, G. E., & Bradley, D. N. (2010). Trouble with diffusion: Reassessing hillslope erosion laws with a particle-based model. *Journal of Geophysical Research*, *115*, F00A10. <https://doi.org/10.1029/2009JF001264>